


Impact of hydraulic tortuosity on microporous and nanoporous media flowShiwani Singh ^{*}*Mathematics Institute, University of Warwick, Coventry CV4 7AL, United Kingdom*

(Received 16 October 2023; accepted 22 January 2024; published 23 February 2024)

Using two-dimensional porous structures made up of homogeneously arranged solid obstacles, we examine the effects of rarefaction on the hydraulic tortuosity in the slip and early transition flow regimes via extended lattice Boltzmann method. We observed that modification in either the obstacle's arrangement or the porosity led to a power-law relation between the porosity-tortuosity. Along with this, we also found that in the slip-flow regime, the exponent of this relation contains the effect of finite Knudsen number (Kn). In addition, we observed that on properly scaling Kn with porosity and hydraulic tortuosity, a generalized correlation can be obtained for apparent permeability.

DOI: [10.1103/PhysRevE.109.025106](https://doi.org/10.1103/PhysRevE.109.025106)**I. INTRODUCTION**

Numerous scientific and engineering applications, including water percolating through soils, gas transportation, CO₂ sequestration, oil extraction with or without polymer flooding, and a host of others can benefit from an understanding of the transportation mechanisms and fluid flow across porous media [1–4]. Porous media are made up of a solid matrix of material that is filled by a network of void spaces (pores) containing fluid and are connected by throats that are significantly smaller in size. One of the main physical properties of interest is the permeability of a porous material which measures its ability to allow fluids (gas or liquid) to flow through it. Apart from porosity, which is defined as the percentage of a porous sample that is occupied by pore space, permeability also depends on the geometry and structure of the pores [1,5,6].

Depending on the geometry and the location of the pores, the actual path taken by the fluid can be very complicated or tortuous. Therefore, a parameter, hydraulic tortuosity (T) was introduced to take care of complicated transport paths in a comprehensive manner [1,7]. Hydraulic tortuosity can be understood as the ratio of the average length of true flow routes to the system's length in the direction of the macroscopic flow. The optimal way to calculate this ratio would be to take the mean flow length from a weighted average of the streamline, however, if the geometry is too complicated, it would not be feasible [2,8]. To overcome this limitation, Koponen *et al.* [7] and Duda *et al.* [9] proposed a straightforward formula for T as a ratio of the mean pore-scale velocity magnitude over the mean of the pore-scale velocity along the main flow direction, which is extremely helpful in the situation of arbitrary geometry.

Furthermore, the emergence of unconventional energy sources, like ultratight gas reservoirs within shale rocks, have shown great potential towards mitigating the world energy crisis [10,11]. Shale rocks are highly tortuous and are made up of fine-grained material which contains pores in the nanoscale size range. At this scale, where the mean-free path of gas molecules becomes equal to or greater than the characteristic flow length within ultratight rocks, the rarefaction effects starts to emerge. The Knudsen number Kn, or the ratio of the mean-free route of gas molecules to the typical flow length, indicates the degree of rarefaction. The fluid behavior can be separated into four primary categories based on the Kn value: continuum flow regime with $Kn < 0.001$, slip flow regime with $0.001 < Kn < 0.1$, transition flow regime with $0.1 < Kn < 10$, and free molecular flow regime with $Kn > 10$. Contrary to what is predicted by Darcy's law in continuum flow regime, rarefaction effect cause gas permeability (apparent) to increase as the pore size decreases. Klinkenberg claimed that this increase is caused due to the rise in gas slippage at the solid-fluid interface [12]. Therefore, to precisely predict the reservoir's production capacity and longevity, it becomes unquestionably crucial to investigate the effect of rarefaction on physical parameters like permeability and tortuosity of ultratight porous media.

The goal of this paper is to provide a deeper understanding of the gas transport characteristics and Kn dependency of various physical properties of porous media, including tortuosity, in carefully designed porous media. The setup is designed in a simple way where the circular obstacles are arranged homogeneously between two parallel plates. The porosity is varied by changing the diameter of the obstacle and the tortuosity is altered by changing the location of next-nearest obstacle. As a simulation technique, we used the lattice Boltzmann (LB) method which has not only proven to be a useful tool for simulating Newtonian continuum hydrodynamics [13–17] but also been successfully extended for flows beyond Navier-Stokes in the past few years, particularly to nonequilibrium (finite Kn) flows. The extended LB method utilizes either a regularization (REG) procedure [18–20] or an appropriate multirelaxation time model [21,22] in

^{*}singh.shiwani@gmail.com

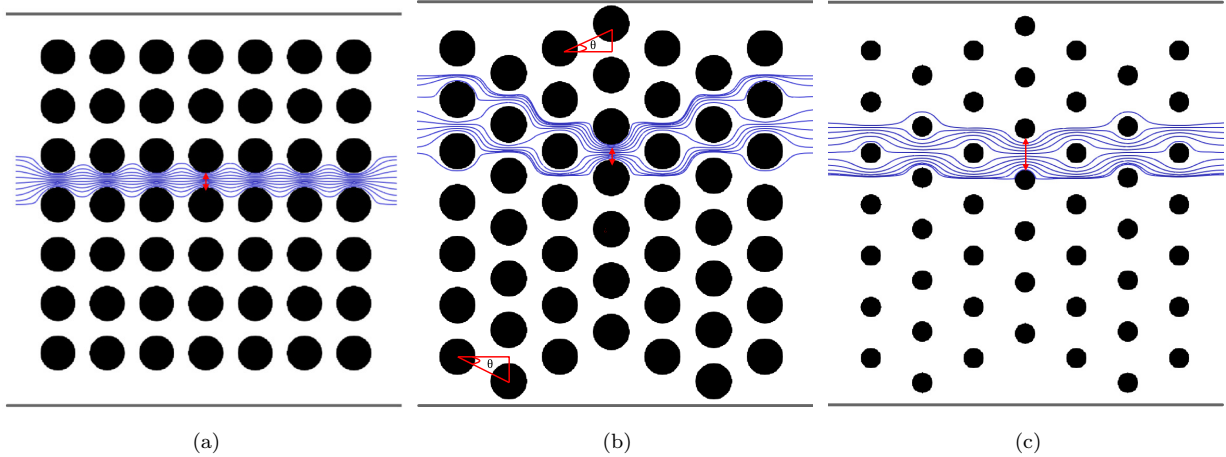


FIG. 1. Schematic of representative porous media designed as an array of circular obstacle in two dimensions. (a) θ_0 , $\phi = 0.75$, (b) θ_6 , $\phi = 0.75$, and (c) θ_6 , $\phi = 0.90$.

combination with the kinetic boundary condition (KBC) [23–26]. We also conducted a thorough parametric study with the goal of determining a consistent way to account for the impact of porosity and tortuosity on gas permeability.

Starting from a brief overview of tortuosity and its evaluation technique in Sec. II, the rest of the paper is organized as follows: In Sec. III, the representative porous media setup is detailed and a reference has been made to the simulation technique, the extended LB method, which is detailed later in the Appendix. This is followed by the Kn-dependent flow investigation in Sec. IV where, starting by investigating the local flow profile at various physical parameters like porosity and porous arrangement, we studied the effect of Kn on tortuosity-porosity relation in Sec. IV A. Further, the effect of tortuosity and porosity on gas permeability was studied in Sec. IV B. Finally, the work is summarized and some future aspects of the work are discussed in Sec. V.

II. TORTUOSITY

Hydraulic tortuosity (T) is the ratio of elongation of fluid streamlines due to the presence of obstacles (porous media) to the system size in the case of free flow [2,8]. Therefore, if λ is the mean distance covered by the fluid element and L is the system size in the direction of flow, the hydraulic tortuosity is defined as

$$T = \frac{\lambda}{L}. \quad (1)$$

By this definition, hydraulic tortuosity is always greater than or equal to 1 ($T \geq 1$). It means in a plane channel flow, $T = 1$ since streamlines face no hindrance in the absence of porous material. The value of T rises when tortuosity grows because fluid has to travel farther through porous media. Since T is defined as deviation of the fluid path, it can be calculated using velocity field. Some of the methods used to calculate T focus on the calculation of weighted averages of discrete streamlines [27,28]. Most of these methods will be difficult to apply in complex geometries. However, in the works of Koponen *et al.* [7] and Duda *et al.* [9], the authors came up with a simple approach for the incompressible and

nonreentrant flow to calculate T by using the appropriate averages of pore-scale velocity vector (\mathbf{u}) in the following manner:

$$T = \frac{\langle |\mathbf{u}| \rangle}{\langle |\mathbf{u} \cdot \mathbf{e}_x| \rangle}, \quad (2)$$

where \mathbf{e}_x is the unit vector in the main direction of the flow. Hereafter, in the present paper, we will be using the above-mentioned definition [Eq. (2)], which is now being routinely used to define T [29–33]. A detailed pedagogical review about the approach used in Ref. [9] can be found in Ref. [34].

III. PHYSICAL POROUS MEDIA

In the present paper, we used simple two-dimensional homogeneous geometries constructed by placing circular obstacles in seven rows and seven columns between two parallel plates to study the effect of tortuosity (see Fig. 1). The LB method is used to solve the flow equations. In the recent past, the LB method has emerged as a powerful tool to solve the continuum hydrodynamics [13,15] and, with some physics-inspired refinements, has shown to capture fluids dynamics beyond Navier-Stokes equations [24,25,35]. The details of this refined method are presented in the Appendix.

In the aforementioned geometrical setup, the lattice node which falls on or inside the solid is marked as nodes_S and the ones occupied by fluid are marked node_F. Hence, the calculation of the porosity (ϕ), defined as the volume (area in two dimensions) of void to the total volume (area), is straightforward and is given as

$$\phi = \frac{\sum \text{node}_F}{\sum \text{node}_F + \sum \text{node}_S}. \quad (3)$$

At this point, it is worth introducing Kn, which is the ratio of the molecular mean-free path with respect to character macroscopic length. The Kn can also be represented in terms of kinematic viscosity, η , as $\text{Kn} = \eta/(dc_s)$ where we chose d to be the smallest pore-throat diameter present as the red double arrow in Fig. 1, and c_s is the speed of sound which is explained later in the Appendix, where the LB method is elaborated on alongside with a REG mechanism which filters

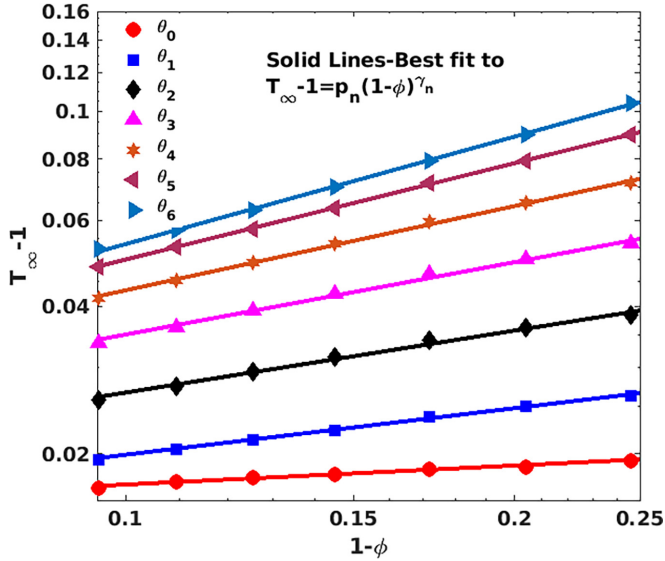


FIG. 2. Tortuosity as a function of porosity for various arrangements in porous media. Solid lines are the best fit to $T - 1 = p_n(1 - \phi)^{\gamma_n}$, where $n(0, 1, \dots, 6)$ defines the alignment.

out the nonhydrodynamic moments and the KBC, which is based on the diffusively reflecting wall. In the recent past, it has been observed that REG and KBC are the crucial ingredients required in the standard LB for the simulation of finite Kn flow [24,25]. The simulations were performed with 500 grid points in each direction, which resulted in 24-38 number grid points representing each pore throat.

Before studying the Kn-dependent rarefaction effects, we focused on the continuum regime to establish the relation between the porosity and tortuosity. Consequently, starting from uniform geometry where distance between the next-nearest circle placed in a row is the same as that of the one placed in a column [Fig. 1(a)], the simplest way to alter tortuosity is to change the arrangement by placing the next-nearest circle at a distance defined by the angle θ as shown in Fig. 1(b). This allowed us to do a controlled study and have insight into how tortuosity increases or decreases with the arrangement of obstacles in the media. We choose the following values of alignments: $[\theta_0, \theta_1, \theta_2, \theta_3, \theta_4, \theta_5, \theta_6] = [0, 5.5^\circ, 9.162^\circ, 10.45^\circ, 14.47^\circ, 17.88^\circ, 21.96^\circ, 25.82^\circ]$. The streamlines passing through the pore throat, present nearly at the middle of the domain, marked with a red double arrow, shows that keeping the porosity the same, tortuosity appears to increase with θ [see Figs. 1(a) and 1(b)]. In Fig. 1(c), we kept the alignment (θ) the same as that of Fig. 1(b) but increased the porosity which resulted in an obvious decrease in tortuosity. Recall, as defined earlier, the larger the average length of streamlines, the larger the tortuosity. To calculate the absolute tortuosity, T_∞ , for each porous configuration in the limit of $\text{Kn} \rightarrow 0$, we extrapolated the tortuosity (T) calculated within the range of $\text{Kn} = 10^{-1}$ to $\text{Kn} = 10^{-3}$ and chose the value at $\text{Kn} = 10^{-7}$ as T_∞ .

Figure 2 represents the absolute tortuosity (T_∞) as a function of porosity for large to medium porosity ranging from 0.90 to 0.75 for all seven alignments (θ_0 to θ_6). First, the figure shows the obvious trend that with increase in porosity,

tortuosity decreases for every configuration. Second, the log-log plot between $T_\infty - 1$ and $1 - \phi$ clearly shows a power-law behavior with the exponent as $[\gamma^0, \gamma^1, \gamma^2, \gamma^3, \gamma^4, \gamma^5, \gamma^6] = [0.1286, 0.3153, 0.4199, 0.4902, 0.5706, 0.6530, 0.7279]$ and constants as $[p_0, p_1, p_2, p_3, p_4, p_5, p_6] = [0.0233, 0.0412, 0.0702, 0.1084, 0.1606, 0.2243, 0.2866]$ (see Fig. 2). This is an empirical relationship, however, it is in agreement with the two-dimensional flow with randomly distributed square obstacles as used by Duda *et al.* [9] for large porosity (<0.8), which also showed a power-law behavior as $T - 1 \sim (1 - \phi)^\gamma$, however, their exponent (γ) was $1/2$.

IV. FLOW AT FINITE KNUDSEN NUMBER

Tortuosity and permeability are two important properties that influence the passage of fluid through a porous media. In the subsequent sections, we will investigate the effect of rarefaction on these two properties. However, first it would also be interesting to observe the behavior of the local velocity in different porous arrangements. Therefore, in Fig. 3, we plotted steady-state streamlines at different Kn for porosities, $\phi = 0.75$ and $\phi = 0.90$, and at pore alignments, θ_0 and θ_6 . The scale for the magnitude of streamlines in all cases has been kept the same to show a relative difference between all the considered arrangements. From Fig. 3, we can make the following observations:

- (1) For a given porosity (ϕ), the flow takes a more tortuous path as the uniformity of the obstacles decreases (i.e., from θ_0 to θ_6) at every Kn.
- (2) In the current configuration, when porosity rises, the pore throat widens, facilitating fluid flow across the porous medium. As a result, the velocity inside the pore-throat increased as the ϕ value increased.
- (3) However, due to Knudsen diffusion, there is a nonzero fluid velocity at solid barriers, which causes the velocity inside the pore throat to grow with increasing Kn in all situations.

A. Effect of finite Kn on tortuosity

Hydraulic tortuosity (T) is the measure of the average fluid streamline length in a porous medium versus system length of obstacle-free flow and, as defined in Eq. (1), can be calculated using appropriate averages of the velocity field component. This makes T a flow-dependent observable. Therefore, any effects of rarefaction that appear on the velocity field, such as increment of slip velocity with Kn, also have a significant effect on T .

To investigate this effect, we computed the value of T as a function of porosity, ϕ , with different Kn for all the arrangements of the porous medium, θ_0 - θ_6 which again shows a power-law behavior, however, with a different exponent (Kn dependent), as shown in Fig. 4. When Kn rises, the slip velocity makes it easier for fluid to move through the pores, which causes a concomitant decrease in the hydraulic tortuosity. This behavior is clearly reflected in Fig. 4. To fully contain the Kn dependency of hydraulic tortuosity in the exponent of the power-law behavior, we plotted the $T - 1$ and $1 - \phi$ with the best fitted lines to the function $T - 1 = p_n(1 - \phi)^{\gamma_n + f_n(\text{Kn})}$ in Fig. 4, where $n(0, 1, 2, \dots, 6)$ dictates the pore arrangement. Here, the values of γ_n and p_n are the same as those

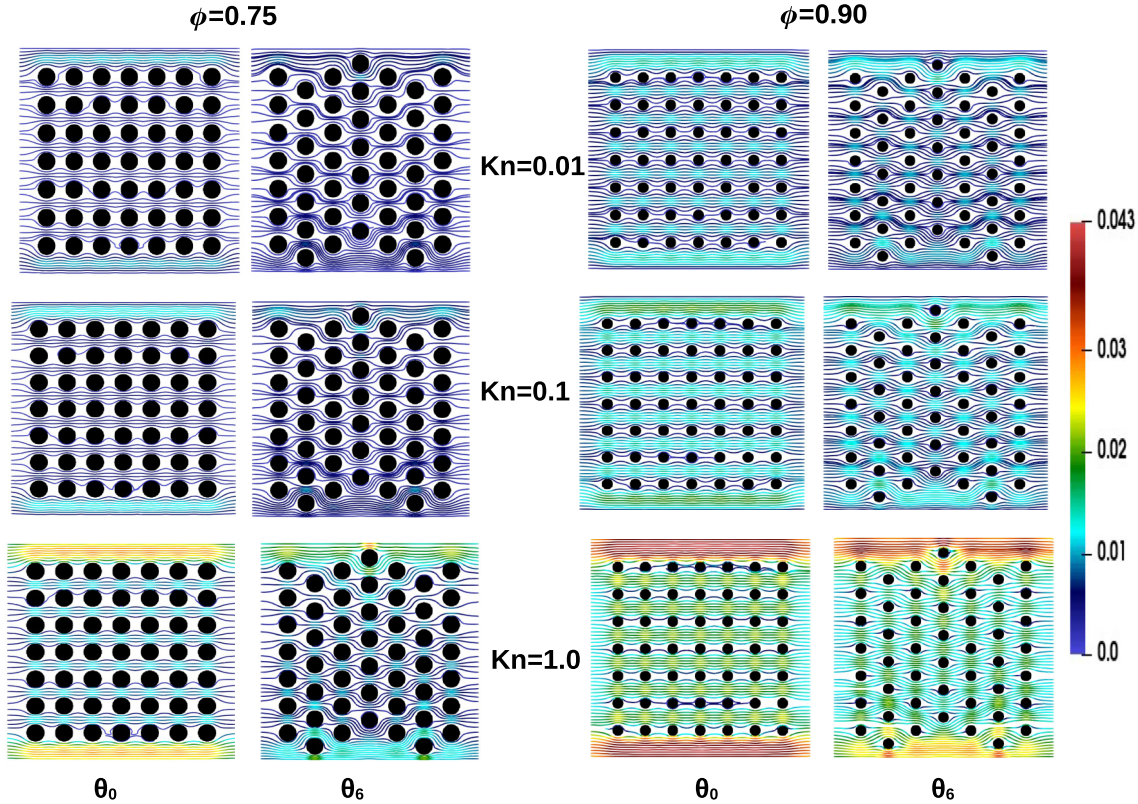


FIG. 3. Steady-state velocity streamlines for porosity, $\phi = 0.75$ and $\phi = 0.90$, porous arrangement, θ_0 and θ_6 , and at $\text{Kn} = 0.01$, $\text{Kn} = 0.1$, and $\text{Kn} = 1.0$.

assessed in Sec. III (Fig. 2). Changing Kn while maintaining the same configuration demonstrates that f_n is an increasing function of Kn because, as Kn rises, the exponent of the power law rises as well. Figure 4 also shows that the exponent in the early-transition phase (bottom few lines in each figure) appears to change less profoundly with changing Kn as the nonuniformity between the pores increases from Fig. 4(a) (θ_1) to Fig. 4(b) (θ_3) and eventually to Fig. 4(c) (θ_6). This shows that when Kn is increased at high nonuniformity, there is less of an effect on physical attributes. In other words, the effect of rarefaction in early transition regime is diminished by higher nonuniformity. But this can also be a result of a technical problem associated with the method. It has been shown in earlier research that a LB model with REG and a diffuse

wall KBC (as used in the current paper) performs admirably well in the slip-flow regime and near the early-transition flow. However, to take into account the flow beyond this limit, one must utilize a higher order lattice (HOL), according to Ref. [24].

Furthermore, to investigate the behavior of f_n with respect to Kn , we plotted f_n as a function of Kn (see Fig. 5) which firstly indicate that f_n is indeed an increasing function of Kn for all the porous arrangements. However, in the slip regime ($0.001 < \text{Kn} < 0.1$), $f_n \sim \text{Kn}^{0.6}$ (see the inset of Fig. 5). This suggests that there exists a consistent dependence of Kn on the tortuosity-porosity relation, at least in the slip flow regime for the porous setup used here, as $T - 1 \sim (1 - \phi)^{(\gamma_n + \text{Kn}^{0.6})}$.

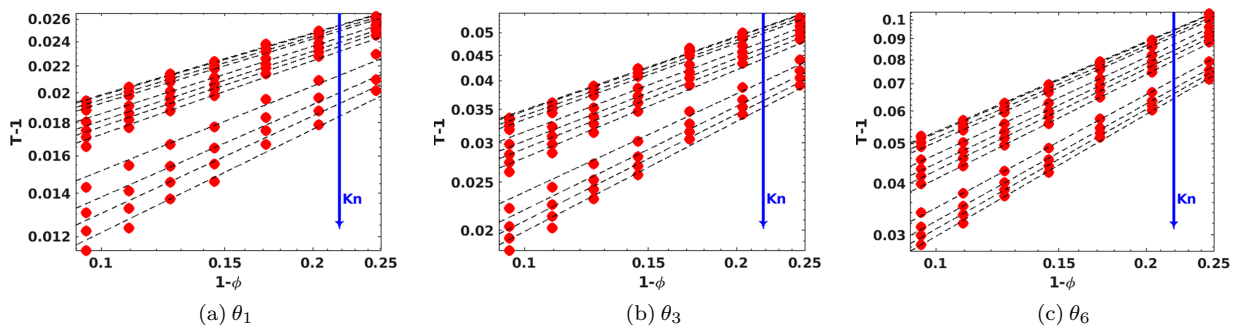


FIG. 4. Tortuosity as a function porosity at pore alignment θ_1 , θ_3 , and θ_6 with varying Kn . Dashed lines are the best fit to the function $T - 1 = p_n(1 - \phi)^{(\gamma_n + f_n(\text{Kn}))}$, where the value of $n(0, 1, 2, \dots, 6)$ depends on the porous arrangement.

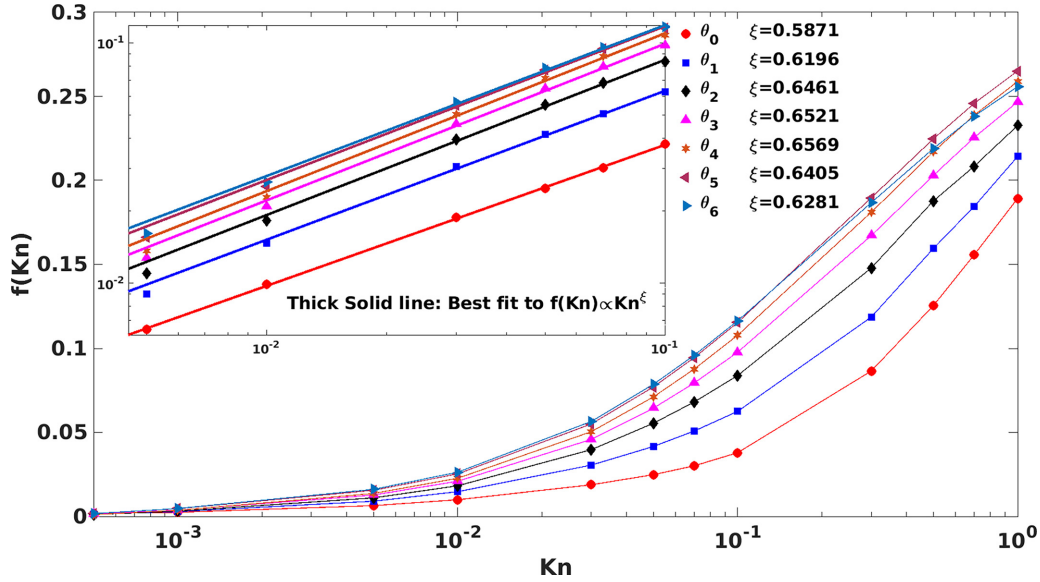


FIG. 5. The Kn-dependent addition in the exponent of power-law behavior, f_n , for various Kn. Here $n(0, 1, \dots, 6)$ describes the alignment of porous arrangement. The inset magnifies the slip-flow regime, which shows that $f(Kn) \sim Kn^{0.6}$.

B. Effect of finite Kn on permeability

One of the physical quantities of interest for the flow inside highly permeable porous media is the absolute permeability (κ_∞), which is obtained by calculating the flux (Q) at different pressure drops (or by adjusting the body force values) in the following manner:

$$\kappa_\infty = \frac{Q\eta}{\rho g}, \quad (4)$$

where η is the dynamic viscosity, g is the body force, and ρ is the density of the fluid. Permeability is a crucial element in determining the transport capacity of porous media. However, in unconventional reservoirs, such as ultratight pores of shale rock, despite the presumption of absolute permeability being very low, experiments observed that apparent gas permeability (AGP) (κ) is much higher than κ_∞ . Furthermore, the idea that the rise in gas slippage at the solid-fluid interface is to blame for the increased permeability was put forward by Klinkenberg, who suggested the permeability correction factor (PCF), which is defined as the ratio of apparent permeability (κ) to absolute permeability (κ_∞), to be a linear function of Kn as

$$\frac{\kappa}{\kappa_\infty} = 1 + 4Kn. \quad (5)$$

Beskok and Karniadakis [36] further proposed a second-order correlation that can be used to describe all four fluid flow regimes and is given as

$$\frac{\kappa}{\kappa_\infty} = [1 + \alpha(Kn)Kn] \left(1 + \frac{4Kn}{1 - bKn} \right), \quad (6)$$

where slip coefficient b equals -1 for slip flow and $\alpha(Kn)$ is the rarefaction coefficient. The expression for $\alpha(Kn)$ is somewhat complex, but Civan [37] later suggested one (Beskok and Karniadakis-Civan's correlation) that is considerably more

straightforward:

$$\alpha(Kn) = \frac{1.358}{1 + 0.170Kn^{-0.4348}}. \quad (7)$$

In addition, Civan [37] suggested that in the slip-flow regime, $\alpha(Kn)$ can also be neglected, making PCF take the following form:

$$\frac{\kappa}{\kappa_\infty} = \left(1 + \frac{4Kn}{1 + Kn} \right). \quad (8)$$

Since up-scaled equations that predict the gas output and longevity of gas wells heavily rely on the AGP at the representative elementary volume scale, it is essential to accurately evaluate AGP. For this reason, we first presented the PCF of different porous media by varying the alignment at fixed porosity (Fig. 6) and then varied the porosity while keeping the alignment unchanged (Fig. 7). To calculate the absolute permeability (κ_∞) for each setup, we extrapolated the permeability calculated within the range from $Kn = 10^{-3}$ to $Kn = 10^{-1}$ and chose the value at $Kn = 10^{-7}$ as κ_∞ . When the porosity is low ($\phi = 0.75$), as shown in Fig. 6(a), the setup with more nonuniformly distributed porous media shows a slightly higher value of PCF over the range of Kn. However, as the porosity is increased to higher values as shown in Figs. 6(b) ($\phi = 0.83$) and 6(c) ($\phi = 0.90$), the PCF starts to overlap onto each other for all the alignments. Likewise, in Fig. 7, we kept the alignment [uniformity (nonuniformity)] of distributed porous media fixed and varied the porosity. In this case, we observed that as Kn is increased (especially in the early transition regime) in all the alignments, the PCF for low porosity has a higher value in comparison to the one with higher porosity. Additionally, this difference becomes more prominent as the dispersion of porous media is further increased from θ_3 to θ_6 . One reason for this behavior at the macroscale level could be that in less porous media, the disturbance caused by one barrier propagates over a smaller distance and interacts with other obstacles before

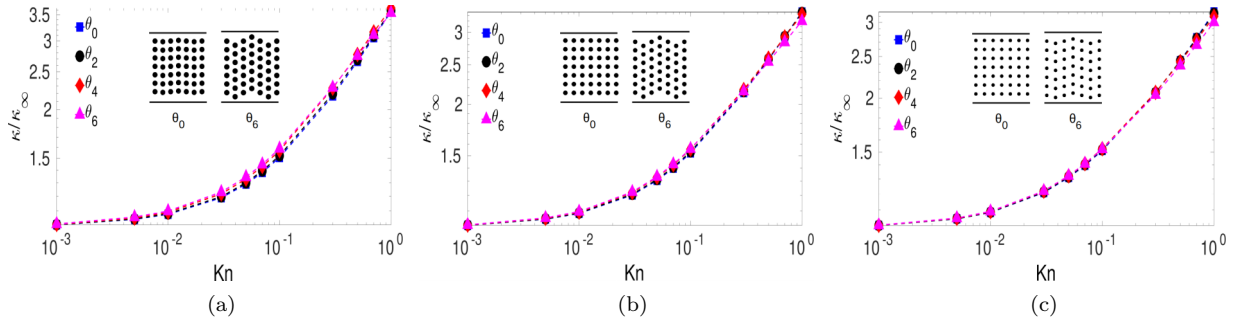


FIG. 6. The permeability correction factor (PCF) as a function of Kn at fixed porosity and varying alignments. (a) $\phi = 0.75$, (b) $\phi = 0.83$, and (c) $\phi = 0.90$.

getting completely dispersed. The hydrodynamic disturbance may, however, tend to fade out or average out in highly porous media before encountering another barrier. This causes different kinds of fluid-solid interactions in addition to slip effect, which could change the magnitude of the velocity field. At the molecular level, large pores with high porosity have a lower rarefaction impact than smaller pores with low porosity because, after colliding inside one pore's throat, the gas molecule must travel a greater distance before colliding with another obstruction in highly porous medium as compared to one with small porosity. Overall, Figs. 6 and 7 led us to the conclusion that, in the current porous setting, porosity has a greater impact on PCF than does nonuniformity (alignment) of porous material, which is one of the factors in determining the tortuosity of the material.

In recent studies, the direct simulation Monte Carlo approach was employed to demonstrate that even for complicated porous structures, the apparent permeability of a porous media can be predicted through the Klinkenberg correlations using fundamental and measurable descriptors of the pore structure [38–41]. This can be accomplished by scaling Kn with an appropriate function of porosity and tortuosity, as suggested by Wu *et al.* [39], or by using an effective pore size that is determined by porosity and tortuosity [40], as it was noticed that using such arguments, the PCF for different porosity and pore structures is found to collapse onto one curve. In a similar manner, we identified one such empirical function, $g = \phi/T^2$, to determine an effective Knudsen number (Kn^*) for the current collection of porous media, given as $\text{Kn}^* = \text{Kn}/g$. This can be inferred indirectly as rescaling of the pore size using parameters related to pore structure, porosity, and pore scale flow, hydraulic tortuosity (T). In

Fig. 8, the PCF is plotted with respect to the effective Knudsen number Kn^* . The figure shows that for all the geometries (chosen at random), the PCF lies almost entirely along a single line. Figure 8 further demonstrates that the PCF and the three proposed correlations—Klinkenberg [Eq. (5)] [12], Beskok and Karniadakis-Civan [Eq. (6)] [36,37], and Civan [Eq. (8)] [37]—are in fair agreement up until the slip-flow regime. However, in the early transition regime, the best agreement is with Civan [37], which was initially suggested for the flow close to slip regime. Figure 3 illustrates that a generalized correlation can be obtained up until the early transition regime with an appropriate effective Knudsen number. It is worth mentioning at this point that in most of the experiments including Klinkenberg's [12], the general expression for the AGP is obtained by employing a straightforward setup, such as flow through a straight capillary by ignoring the effect of tortuosity. Consequently, in intricately organized porous media, one should expect a departure from these predictions. Nevertheless, a technical issue could also be the cause of the divergence of these predictions at high Kn number flow. We want to reiterate that it has been postulated that at-least three primary components are required to extend a simple Bhatnager-Gross-Krook (BGK) approximation based LB beyond Navier-Stokes: KBC, REG, and HOL [24]. However, in this paper, we made use of the fact established by Ref. [25] that the combination of REG and KBC works effectively in two-dimensional flow up until the early transition regime, without invoking HOL. It is expected that when the Kn rises beyond the transition regime, the HOL will become more significant. Therefore, we plan to do a thorough investigation to ascertain the appropriate order of lattices required for the given setup for very high- Kn flows.

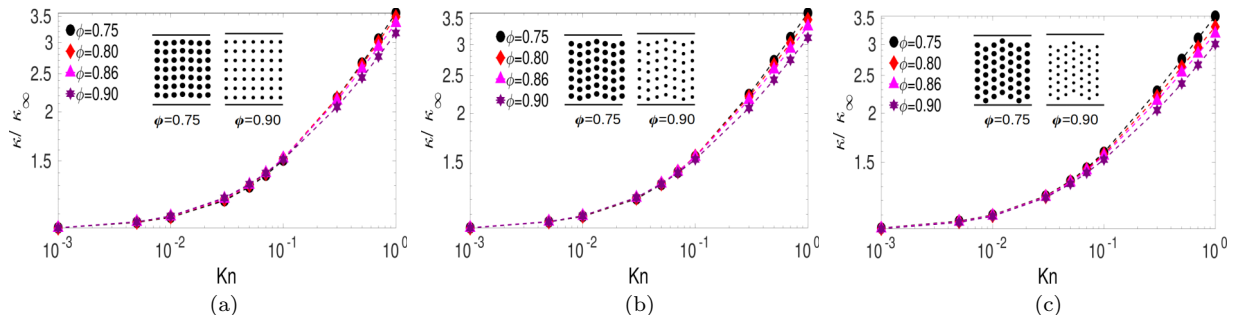


FIG. 7. The permeability correction factor (PCF) as a function of Kn at fixed alignment and varying porosity. (a) θ_0 , (b) θ_3 , and (c) θ_6 .

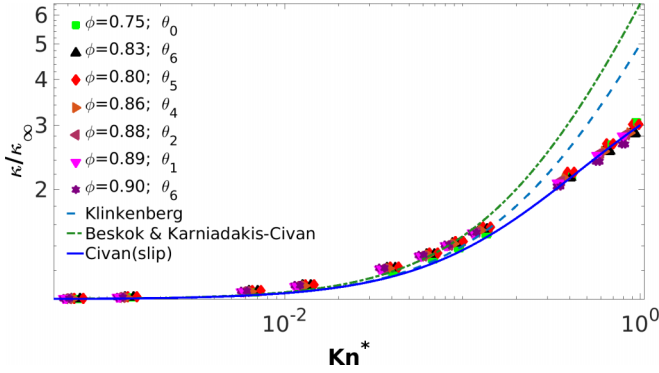


FIG. 8. The permeability correction factor (PCF) as a function of an effective Kn^* at randomly selected porous media configuration. The first-order correlation by Klinkenberg [Eq. (5)] [12], the second-order correlation given by Beskok and Karniadakis-Civan [Eq. (6)] [36,37], and the correlation in the slip flow regime suggested by Civan [Eq. (8)] [37] are also presented as a reference.

V. CONCLUSION AND OUTLOOK

We investigated the gas-transport characteristics flowing across two-dimensional porous medium containing micro- and nanopores for moderate to high porosities of $0.75 < \phi < 0.90$ from the continuum to early-transition regimes in a systematic manner using the extended LB method with a focus on two physical parameters of the flow namely, tortuosity and permeability. *A priori*, it is not obvious that tortuosity and porosity, in general, have a universal relationship. However, such correlation can arise, at least for some porous material types. With this aim, we explored the gas transport in homogeneously arranged porous media, which showed an empirical power-law behavior between the two as $T - 1 \sim (1 - \phi)^\nu$. An further investigation across various Kn shows that, in the slip-flow regime, the Kn dependency alters the exponent of the power as $T - 1 \sim (1 - \phi)^{\nu+f_n}$ with $f_n \sim \text{Kn}^{0.6}$, giving a generalized relation between the two.

In addition, we discovered that PCF with respect to Kn , which appears as a result of rarefaction, falls nearly on one single line up until early transition regime, indicating a generalized correlation, with appropriate scaling of Kn with parameters like porosity and hydraulic tortuosity. Moreover, how the Kn should be properly scaled using ϕ and T in a heterogeneous and tortuous environment may also be crucial to examine other phenomena such as the dispersive transport of a scalar through complex media with pore size ranging from micro- to nanometers [42]. It should be emphasized that the implementation of the diffuse wall boundary condition, which requires wall normals, was simple due to the simplicity of the current 2D setup formed by arranging circular obstacles in a homogeneous pattern at different orientations. In most cases, the flow characteristics of three-dimensional flows are only partially represented by two-dimensional flow in porous media. On top of that, the distribution of pores in a real rock is highly heterogeneous and tortuous. Therefore, it will be interesting to observe how the aforementioned exponent varies not only in two-dimensional flow inside heterogeneously structured porous media but also in analogous three-dimensional flow. Therefore, in the future, we will explore the fluid flow in

a realistic low-porosity geometry of natural rock imaged by a multislice micro-CT scanner [43,44] by utilizing a boundary condition that was more practical for such a scenario and does not require calculating wall normals as proposed in Ref. [25].

ACKNOWLEDGMENTS

S.S. acknowledges the financial support by the Leverhulme Trust (ECF-2019-100). S.S. also acknowledges the use of the Scientific Computing Research Technology Platform and associated support services at the University of Warwick, in the completion of this paper.

APPENDIX: LATTICE BOLTZMANN METHOD

The conventional LBM framework is based on the Boltzmann equation with the single relaxation approximation, also known as the BGK approximation [45]. The discrete form of such an equation requires a set of discrete populations $f = \{f_i\}$ and corresponding to which there exists a predefined discrete velocities c_i ($i = 1, \dots, N$) [13,15] and has the following form:

$$f_i(\mathbf{x} + \mathbf{c}_i \Delta t, t + \Delta t) = f_i(\mathbf{x}, t) + \Omega_i(f) + \Delta t F_i. \quad (\text{A1})$$

Here, F_i corresponds to the i th component of external force and the BGK collision approximation, $\Omega_i(f)$, given as

$$\Omega_i(f) = \frac{\Delta t}{\tau} (f_i^{\text{eq}} - f_i(\mathbf{x}, t)), \quad (\text{A2})$$

dictates the relaxation of distribution function to an equilibrium Maxwell-Boltzmann function, f^{eq} , as given in Eq. (A3), at the rate of τ^{-1} .

$$f_i^{\text{eq}} = w_i \rho \left[1 + \frac{\mathbf{c}_i \cdot \mathbf{u}}{c_s^2} + \frac{(\mathbf{c}_i \cdot \mathbf{u})^2}{2 c_s^4} - \frac{(\mathbf{u} \cdot \mathbf{u})}{2 c_s^2} \right]. \quad (\text{A3})$$

The two-dimensional model (D2Q9) which is chosen for the present paper has the following nine discrete velocities:

$$c_i = \begin{cases} (0, 0) & \text{if } i = 0 \\ \left(\cos \frac{(i-1)\pi}{4}, \sin \frac{(i-1)\pi}{4} \right) & \text{if } i = 1, 2, 3, 4 \\ \sqrt{2} \left(\cos \frac{(i-1)\pi}{4}, \sin \frac{(i-1)\pi}{4} \right) & \text{if } i = 5, 6, 7, 8, \end{cases} \quad (\text{A4})$$

with the corresponding weights as

$$w_i = \begin{cases} \frac{4}{9} & \text{for } i = 0 \\ \frac{1}{9} & \text{for } i = 1, 2, 3, 4 \\ \frac{1}{36} & \text{for } i = 5, 6, 7, 8. \end{cases} \quad (\text{A5})$$

The lattice sound speed c_s that appeared in Eq. (A3) is related to the magnitude of discrete velocity as $c^2 = 3c_s^2$. As mentioned earlier, the Kn for the flow is $\eta/(dc_s)$, with the kinematic viscosity being defined as $\eta = c_s^2(\tau - \delta t/2)$ and d being the smallest pore-throat diameter. Hence, the Kn can be controlled by varying the viscosity through the relaxation time τ for a given setup. The relevant hydrodynamic macroscopic moments, like density (ρ), momentum density ($\rho \mathbf{u}$), and momentum flux ($\mathbf{\Pi}$) can be obtained by linear weighted sums as $\rho(\mathbf{x}, t) = \sum_i f_i$, $\rho(\mathbf{x}, t) \mathbf{u}(\mathbf{x}, t) = \sum_i f_i c_i$, and $\mathbf{\Pi}(\mathbf{x}, t) = \sum_i f_i (\mathbf{c}_i c_i - c_s^2 \delta)$, respectively, with δ being the identity matrix. Finally, the term F_i in

Eq. (A1), which is the i th component of the body force, is given as [46]

$$F_i = w_i \rho \left[\frac{\mathbf{g} \cdot \mathbf{c}_i}{c_s^2} + \frac{(\mathbf{g}\mathbf{u} + \mathbf{u}\mathbf{g})}{2c_s^2} : (\mathbf{c}_i \mathbf{c}_i - c_s^2 \delta) \right], \quad (\text{A6})$$

where \mathbf{g} is the constant acceleration vector. In the subsequent section, we will briefly discuss a REG scheme which was introduced to filter out the nonphysical effect from finite Kn flow.

1. Regularization scheme

Initially proposed to resolve the issue of stability of high viscous flows, the REG process, as introduced by Chen and coworkers [18,19] and Latt and Chopard [20], turns out to be one of the major ingredients for the finite Kn flow [24] in the LB framework. In the REG process, nonhydrodynamic (ghost) modes are filtered out by dividing the poststreaming distribution function into two parts as

$$f_i = f_i^{\text{eq}} + f_i^{\text{neq}}. \quad (\text{A7})$$

The information about the hydrodynamic modes is contained in f_i^{eq} and to remove the information of nonhydrodynamic modes from f_i^{neq} , it is converted into a new distribution function f_i^{Reg} which is then defined in terms of hydrodynamic moments (ρ , \mathbf{u} , $\mathbf{\Pi}$) and has the following discrete form:

$$f_i^{\text{Reg}} = \frac{w_i}{2c_s^4} (\mathbf{c}_i \mathbf{c}_i - c_s^2 \delta) : \mathbf{\Pi}^{\text{neq}}, \quad (\text{A8})$$

where $\mathbf{\Pi}^{\text{neq}}$ is the nonequilibrium part of momentum flux and is given as $\mathbf{\Pi}^{\text{neq}} = \sum_i f_i^{\text{neq}} (\mathbf{c}_i \mathbf{c}_i - c_s^2 \delta)$. The streaming step of LB method takes the following form after the REG process:

$$f_i(\mathbf{x} + \mathbf{c} \Delta t, t + \Delta t) = f_i^{\text{eq}} + \left(1 - \frac{\Delta t}{\tau}\right) f_i^{\text{Reg}} + \Delta t F_i. \quad (\text{A9})$$

2. Kinetic boundary condition

The no-slip boundary conditions based on a bounce-back mechanism, where the directions of the incoming distribution functions are simply reversed when it encounters the boundary node, as the name suggests, fails to uncover the slip velocity at the boundary at finite Kn. To overcome this shortcoming of the method, a diffusively reflecting solid wall boundary condition was introduced by Ansumali and Karlin [23]. Based on kinetic

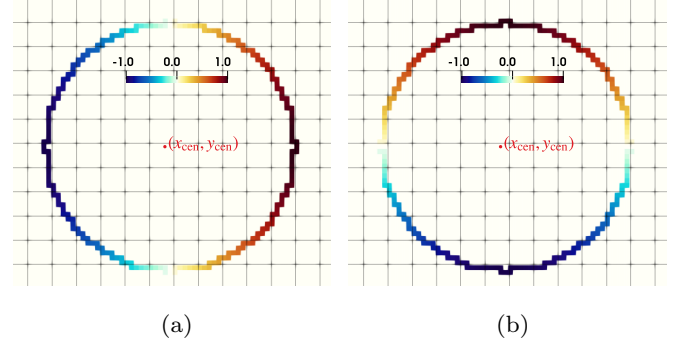


FIG. 9. Unit normals at the solid boundaries.

theory interpretation, this boundary condition redistributes the population coming towards the wall in such a way that mass balance and normal-flux conditions are fulfilled. In the discrete sense, the distribution function at the boundary (wall) takes the following form:

$$f_i(\mathbf{x}_w, t) = K f_i^{\text{eq}}(\rho, \mathbf{u}_w), \quad (\text{A10})$$

where subscript w denotes the wall and

$$K = \frac{\sum_{\mathbf{c}_i \cdot \mathbf{n} < 0} |(\mathbf{c}_i - \mathbf{u}_w) \cdot \mathbf{n}| f_i}{\sum_{\mathbf{c}_i \cdot \mathbf{n} > 0} |(\mathbf{c}_i - \mathbf{u}_w) \cdot \mathbf{n}| f_i^{\text{eq}}(\rho, \mathbf{u}_w)}, \quad (\text{A11})$$

with \mathbf{n} being the unit normal direction. The term K can be understood as the ratio of outgoing flux from the wall and incoming equilibrium flux coming towards the wall. When the boundaries are stationary ($\mathbf{u}_w = 0$), the term K can be written as

$$K = \frac{\sum_{A_i < 0} |A_i| f_i}{\sum_{A_i > 0} |A_i| f_i^{\text{eq}}}, \quad (\text{A12})$$

with $A_i = c_{ix} n_x + c_{iy} n_y$. To implement this boundary condition, one needs the information of unit normals at the boundaries. Figures 9(a) and 9(b), respectively, represent the unit normals in the x direction, n_x , and the same in the y direction, n_y [25,26] for a circular obstacle. In the present paper, the normals for an individual circle with center $(x_{\text{cen}}, y_{\text{cen}})$ are calculated as

$$\hat{\mathbf{n}} = \frac{\mathbf{x} - \mathbf{x}_{\text{cen}}}{|\mathbf{x} - \mathbf{x}_{\text{cen}}|}. \quad (\text{A13})$$

-
- [1] J. Bear, *Dynamics of Fluids in Porous Media* (Dover Publication, Inc., New York, 1972).
- [2] B. Ghanbarian, A. G. Hunt, R. P. Ewing, and M. Sahimi, Tortuosity in porous media: A critical review, *Soil Science Soc. Am. J.* **77**, 1461 (2013).
- [3] B. Metz, O. Davidson, H. C. De Coninck, M. Loos, and L. Meyer, *IPCC Special Report on Carbon Dioxide Capture and Storage* (Cambridge University Press, Cambridge, 2005).
- [4] L. W. Lake, *Enhanced Oil Recovery* (Prentice Hall, Englewood Cliffs, New Jersey, 1989).
- [5] P. C. Carman, Fluid flow through a granular bed, *Trans. Inst. Chem. Eng. London* **15**, 150 (1937).
- [6] F. A. L. Dullien, *Porous Media: Fluid Transport and Pore Structure* (Academic Press, Inc., San Diego, California, 2012).
- [7] A. Koponen, M. Kataja, and J. V. Timonen, Tortuous flow in porous media, *Phys. Rev. E* **54**, 406 (1996).
- [8] M. Matyka, A. Khalili, and Z. Koza, Tortuosity-porosity relation in porous media flow, *Phys. Rev. E* **78**, 026306 (2008).
- [9] A. Duda, Z. Koza, and M. Matyka, Hydraulic tortuosity in arbitrary porous media flow, *Phys. Rev. E* **84**, 036319 (2011).
- [10] F. Javadpour, D. Fisher, and M. Unsworth, Nanoscale gas flow in shale gas sediments, *J. Can. Pet. Technol.* **46**, 10 (2007).
- [11] C. M. Freeman, G. J. Moridis, and T. A. Blasingame, A numerical study of microscale flow behavior in tight gas and shale gas reservoir systems, *Transp. Porous Media* **90**, 253 (2011).
- [12] L. J. Klinkenberg, *The Permeability of Porous Media to Liquids and Gases*, American Petroleum Institute Drilling and Produc-

- tion Practice Paper (American Petroleum Institute, Washington, DC, 1941), pp. 200–213.
- [13] R. Benzi, S. Succi, and M. Vergassola, The lattice Boltzmann equation: Theory and applications, *Phys. Rep.* **222**, 145 (1992).
- [14] S. Chen and G. D. Doolen, Lattice Boltzmann method for fluid flows, *Annu. Rev. Fluid Mech.* **30**, 329 (1998).
- [15] S. Succi, *The Lattice Boltzmann Equation: For Fluid Dynamics and Beyond* (Clarendon Press, Oxford, 2001).
- [16] C. K. Aidun and J. R. Clausen, Lattice-Boltzmann method for complex flows, *Annu. Rev. Fluid Mech.* **42**, 439 (2010).
- [17] T. Krüger, H. Kusumaatmaja, A. Kuzmin, O. Shardt, G. Silva, and E. M. Viggien, *The Lattice Boltzmann Method: Principles and Practice* (Springer, Cham, Switzerland, 2017).
- [18] Y. Zhou, R. Zhang, I. Staroselsky, H. Chen, W. T. Kim, and M. S. Jhon, Simulation of micro- and nano-scale flows via the lattice Boltzmann method, *Physica A* **362**, 68 (2006).
- [19] R. Zhang, X. Shan, and H. Chen, Efficient kinetic method for fluid simulation beyond the Navier-Stokes equation, *Phys. Rev. E* **74**, 046703 (2006).
- [20] J. Latt and B. Chopard, Lattice Boltzmann method with regularized pre-collision distribution functions, *Math. Comput. Simul.* **72**, 165 (2006).
- [21] S. Tao and Z. Guo, Boundary condition for lattice Boltzmann modeling of microscale gas flows with curved walls in the slip regime, *Phys. Rev. E* **91**, 043305 (2015).
- [22] Z. Guo, J. Qin, and C. Zheng, Generalized second-order slip boundary condition for nonequilibrium gas flows, *Phys. Rev. E* **89**, 013021 (2014).
- [23] S. Ansumali and I. V. Karlin, Kinetic boundary conditions in the lattice Boltzmann method, *Phys. Rev. E* **66**, 026311 (2002).
- [24] A. Montessori, P. Prestinanzi, M. L. Rocca, and S. Succi, Lattice Boltzmann approach for complex nonequilibrium flows, *Phys. Rev. E* **92**, 043308 (2015).
- [25] S. Singh, F. Jiang, and T. Tsuji, Impact of the kinetic boundary condition on porous media flow in the lattice Boltzmann formulation, *Phys. Rev. E* **96**, 013303 (2017).
- [26] S. Singh, F. Jiang, and T. Tsuji, Influence of slip flow at fluid-solid interface upon permeability of natural rock, *Energy Procedia* **114**, 3572 (2017).
- [27] M. A. Knackstedt and X. Zhang, Direct evaluation of length scales and structural parameters associated with flow in porous media, *Phys. Rev. E* **50**, 2134 (1994).
- [28] X. Zhang and M. A. Knackstedt, Direct simulation of electrical and hydraulic tortuosity in porous solids, *Geophys. Res. Lett.* **22**, 2333 (1995).
- [29] M. Icardi, G. Boccardo, D. L. Marchisio, T. Tosco, and R. Sethi, Pore-scale simulation of fluid flow and solute dispersion in three-dimensional porous media, *Phys. Rev. E* **90**, 013032 (2014).
- [30] M. Matyka, J. Golembiewski, and Z. Koza, Power-exponential velocity distributions in disordered porous media, *Phys. Rev. E* **93**, 013110 (2016).
- [31] B. P. Muljadi, M. J. Blunt, A. Q. Raeini, and B. Bijeljic, The impact of porous media heterogeneity on non-Darcy flow behaviour from pore-scale simulation, *Adv. Water Resour.* **95**, 329 (2016).
- [32] A. A. El-Zehairy, M. M. Nezhad, V. Joekar-Niasar, I. Guymmer, N. Kourra, and M. A. Williams, Pore-network modelling of non-Darcy flow through heterogeneous porous media, *Adv. Water Resour.* **131**, 103378 (2019).
- [33] K. M. Graczyk and M. Matyka, Predicting Porosity, permeability, and tortuosity of porous media from images by deep learning, *Sci. Rep.* **10**, 21488 (2020).
- [34] M. Matyka and Z. Koza, How to calculate tortuosity easily? *AIP Conf. Proc.* **1453**, 17 (2012).
- [35] S. Mohammed and T. Reis, Lattice Boltzmann method with moment-based boundary conditions for rarefied flow in the slip regime, *Phys. Rev. E* **104**, 045309 (2021).
- [36] A. Beskok and G. E. Karniadakis, Report: A model for flows in channels, pipes, and ducts at micro and nano scales, *Microscale Thermophys. Eng.* **3**, 43 (1999).
- [37] F. Civan, Effective correlation of apparent gas permeability in tight porous media, *Transp. Porous Media* **82**, 375 (2010).
- [38] L. Wu, H. Liu, J. M. Reese, and Y. Zhang, Non-equilibrium dynamics of dense gas under tight confinement, *J. Fluid Mech.* **794**, 252 (2016).
- [39] L. Wu, M. T. Ho, L. Germanou, X.-J. Gu, C. Liu, K. Xu, and Y. Zhang, On the apparent permeability of porous media in rarefied gas flows, *J. Fluid Mech.* **822**, 398 (2017).
- [40] G. Yang and B. Weigand, Investigation of the Klinkenberg effect in a micro/nanoporous medium by direct simulation Monte Carlo method, *Phys. Rev. Fluids* **3**, 044201 (2018).
- [41] W. Su, M. T. Ho, Y. Zhang, and L. Wu, GSIS: An efficient and accurate numerical method to obtain the apparent gas permeability of porous media, *Comput. Fluids* **206**, 104576 (2020).
- [42] F. J. Meigel, T. Darwent, L. Bastin, L. Goehring, and K. Alim, Dispersive transport dynamics in porous media emerge from local correlations, *Nat. Commun.* **13**, 5885 (2022).
- [43] F. Jiang and T. Tsuji, Changes in pore geometry and relative permeability caused by carbonate precipitation in porous media, *Phys. Rev. E* **90**, 053306 (2014).
- [44] F. Jiang, Y. Guo, T. Tsuji, Y. Kato, M. Shimokawara, L. Esteban, M. Seyyedi, M. Pervukhina, M. Lebedev, and R. Kitamura, Upscaling permeability using multiscale x-ray-CT images with digital rock modeling and deep learning techniques, *Water Resour. Res.* **59**, e2022WR033267 (2023).
- [45] P. L. Bhatnagar, E. P. Gross, and M. Krook, A model for collision processes in gases. I. Small amplitude processes in charged and neutral one-component systems, *Phys. Rev.* **94**, 511 (1954).
- [46] Z. Guo, C. Zheng, and B. Shi, Discrete lattice effects on the forcing term in the lattice Boltzmann method, *Phys. Rev. E* **65**, 046308 (2002).